



Appropriate amount of polyaniline coated Co_3O_4 nanofibers and their excellent electrochemical properties

Jia Lei, Yabo Zhu^{*}, Chao Shi, Qian Xu, Xueyu Tao

School of Materials Science and Engineering, China University of Mining and Technology, Xuzhou, 221116, PR China

ARTICLE INFO

Keywords:

Co_3O_4 nanofibers
 Polyaniline
 Composite
 Electrochemical property

ABSTRACT

Co_3O_4 /PANI composites with different proportion were synthesized by in-situ polymerization method. The morphology of the composites showed that cobalt oxide fibers were wrapped up in polyaniline (PANI). The electrochemical tests showed that Co_3O_4 /PANI (1:5) had the highest specific capacitance of 1124 F g^{-1} among the all samples. Its capacitance retention was up to 82.19% after 2000 charge-discharge cycles at 5 A g^{-1} . Especially, after 5000 cycles, the capacitance retention was 73.97%, showing excellent cycling stability. It was found that the combination of PANI and cobalt oxide fiber in proper proportion was beneficial to the conductivity and ion diffusivity of the system, and was also beneficial to improve the redox efficiency of cobalt oxide. This is synergistic effect, which can bring good electrochemical performance to the system.

1. Introduction

Supercapacitor is an attractive energy storage device [1], which has many advantages in its power density, charge-discharge rate and cyclical stability etc. The electrode material of supercapacitor has an important influence on its performance. At present, a variety of materials were explored for electrode, including conductive polymers [2,3], metal oxides [4,5], carbon materials [6–8] and metal sulfide [9,10].

Co_3O_4 is a fascinating electrode material for lithium batteries, in addition, it is also used in gas sensors, catalysts and capacitors etc. [11, 12] It has been found that Co_3O_4 had a theoretical capacitance up to 3560 F g^{-1} [13]. But nanostructured Co_3O_4 such as nanorods and nanowires [14,15] only showed a lower capacitance because of its poor conductivity and ion mobility. At present, it is a popular idea that cobalt oxide-based composite material can promote the performance of the electrodes through the possible synergy between different components of the composites [16–18]. PANI, as a conductive organic material, if combined with cobalt oxide, may be helpful to improve the conductivity of the system and then improve the capacitance performance [19]. It has been reported that Mn_2O_3 /PANI composite showed the specific capacitance of 719 F g^{-1} [20] and PANI/NiO nanocomposite also reached the specific capacitance of 514 F g^{-1} [21]. These improvements should be related to the synergistic effect [22].

In this paper, a new cobalt oxide/PANI composite is designed. Firstly, cobalt oxide nanofibers are prepared by electrospinning. And

then they are placed in HCl solution and aniline monomer is also added into the solution. After that, the composites of polyaniline coated cobalt oxide fibers can be obtained through in situ polymerization method. The samples with different molar ratio of cobalt oxide to PANI are prepared by controlling the number of aniline monomers. The electrochemical test shows that Co_3O_4 /PANI (1:5) delivers a high specific capacitance and excellent cycle life. The synergistic effect may make an important contribution to the good performance.

2. Experiment

2.1. Preparation of Co_3O_4 /PANI

For preparation of Co_3O_4 nanofibers, $0.8 \text{ g Co}(\text{NO}_3)_2 \cdot 6\text{H}_2\text{O}$ and 2.0 g polyvinylpyrrolidone (PVP) are dissolved in 10 ml N–N dimethylformamide (DMF) and 5 ml $\text{C}_2\text{H}_5\text{OH}$. A homogeneous spun precursor is obtained after 12 h stirring. The electrospinning is carried out under the syringe propulsive pump speed of 0.5 mL h^{-1} and the voltage between the needle and the collection with 15 kV . The obtained products are non-woven fabric, which is heated to $480 \text{ }^\circ\text{C}$ for 3 h to obtain Co_3O_4 nanofibers at last.

For preparation of the composites, 12 mg Co_3O_4 fibers are added into 5 ml 0.5 mol L^{-1} HCl solution, and then dispersed evenly by ultrasound. After that, aniline monomers are added with the molar ratio of 1:3, 1:5, 1:8, 1:10, respectively. And an appropriate amount of ammonium

^{*} Corresponding author.

E-mail address: zhuyabo@163.com (Y. Zhu).

<https://doi.org/10.1016/j.physe.2019.113836>

Received 11 August 2019; Received in revised form 12 November 2019; Accepted 19 November 2019

Available online 20 November 2019

1386-9477/© 2019 Elsevier B.V. All rights reserved.

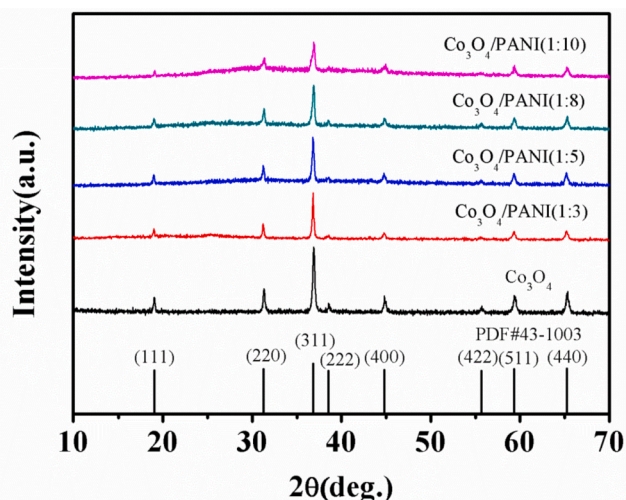


Fig. 1. XRD patterns of Co_3O_4 and $\text{Co}_3\text{O}_4/\text{PANI}$ (1:3, 1:5, 1:8, 1:10).

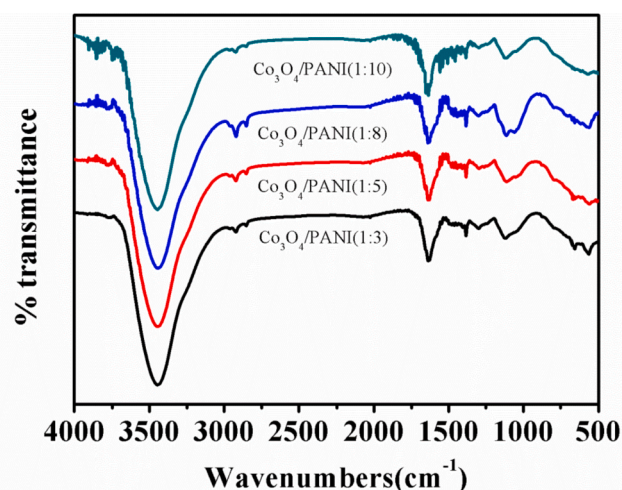


Fig. 2. IR spectra of $\text{Co}_3\text{O}_4/\text{PANI}$ (1:3, 1:5, 1:8, 1:10).

persulfate (APS, the molar ratio of Aniline monomer to APS is 1:1) is added into the above solution. $\text{Co}_3\text{O}_4/\text{PANI}$ composites can be synthesized by in-situ polymerization with stirring in ice bath for 1 h.

2.2. Structure and morphology characterization

The samples are characterized by XRD (D8 Advance), IR (Nicolet iS5), SEM (SU8220), TEM (Tecnai G2 F20), XPS (ESCALAB 250Xi), granularity testing (NanoBrook Omni Zeta Potential Analytical Instruments), BET (MicroActive for ASAP 2460 2.02).

2.3. Electrochemical characterization

The electrochemical tests are performed on CHI660e electrochemical work station. And the prepared samples, platinum foil and Hg/HgO are used as working electrode, counter electrode, and reference electrode, respectively. Cyclic voltammogram (CV) tests are carried out in the voltage range of 0–0.6 V with a scan rate of 10–200 mV s^{-1} . The potential window for galvanostatic charge–discharge (GCD) test is selected with 0–0.5 V, while the current density is selected in the range of 1–20 A g^{-1} . The frequency range of electrochemical impedance spectroscopy (EIS) is 0.01 Hz–100 kHz. The initial potential is open circuit voltage. The charge–discharge cycles are tested by LANHE at 5 A g^{-1} , and the

potential window is 0–0.5 V. Tafel polarization is executed on three-electrode system by electrochemical work station (RST5060F).

The specific capacitance can be calculated by the following formula:

$$C = \frac{I\Delta t}{m\Delta V} \quad (1)$$

In which, I , Δt , m and ΔV are current density, discharge time, the mass of active substance and potential window, respectively.

3. Results and discussions

3.1. X-ray diffraction (XRD)

The XRD results are shown in Fig. 1. The diffraction peaks of all samples at the diffraction angles of 19° , 31.3° , 36.8° , 38.5° , 44.8° , 55.6° , 59.3° and 65.2° are relative to (111), (220), (311), (222), (400), (422), (511), (440) of Co_3O_4 crystal (PDF#43–1003), respectively. It is obvious that the half bandwidth widens with the increase of the amount of PANI in samples, which means more added PANI can lead to the poor crystallinity of Co_3O_4 . On the other hand, there are some weak peaks near 25° in the XRD pattern of the composites, which belong to PANI macromolecular chain.

3.2. Infra-red spectrum (IR)

The Infra-red spectra of the composites are shown in Fig. 2. Obviously, the peaks between 2920 and 2800 cm^{-1} belong to the C–H stretching vibration peaks of benzene rings [23]. The peaks around 1640 and 1383 cm^{-1} are stretching vibration peaks of C=C in the quinonoid rings and benzenoid rings. The two peaks at 1298 and 1112 cm^{-1} are the characteristic peaks related to N atom in PANI. They are assigned to C–N and $-\text{NH}^+$ [24]. The peaks at 650 and 563 cm^{-1} are characteristic peaks related to Co_3O_4 fibers. They are originating from the stretching vibrations of the metal–oxygen bonds [25]. The peak at 563 cm^{-1} is attributed to Co^{3+} in octahedral gap in spinel lattice, and the peak at 650 cm^{-1} originates from Co^{2+} vibration in tetrahedral void. The higher the content of PANI in the sample, the weaker corresponding peaks of 563 and 650 cm^{-1} . Here, the infrared spectra show rich information about the existence of PANI and cobalt oxide.

3.3. Scanning electron microscope (SEM) and transmission electron microscope (TEM)

The morphologies of Co_3O_4 and $\text{Co}_3\text{O}_4/\text{PANI}$ (1:5) are characterized by SEM and TEM, respectively. In Fig. 3a, the SEM picture shows the morphology of Co_3O_4 nanofibers with diameter about 200 nm. Fig. 3b and c shows the morphology of $\text{Co}_3\text{O}_4/\text{PANI}$ (1:5), in which Co_3O_4 fibers are coated by nanoPANI and a spiny structure is formed on the surface. Granularity testing can give a rough estimate of the size of all samples. The results are as shown in Table 1. Obviously, more PANI leads to more aggregation, so the effective diameter increases. Fig. 3d is the TEM of $\text{Co}_3\text{O}_4/\text{PANI}$ (1:5), in which the dark portion is Co_3O_4 fibers and the grey portion is the PANI. The TEM further shows the structure of the composite with fibers wrapped by PANI. Elemental mappings show that PANI is evenly covered on the surface of Co_3O_4 .

3.4. X-ray photoelectron spectroscopy (XPS)

In the XPS of $\text{Co}_3\text{O}_4/\text{PANI}$ (1:5) as shown in Fig. 4a, there are clearly peaks of S 2p, Cl 2p, C 1s, N 1s, O 1s and Co 2p. C and N are the elements of PANI backbone. The sharp peaks locate at 399.4, 399.9 and 401.2 eV correspond to the characteristic peaks of quinine ring, benzene ring and N-atoms of the semiquinone cationic radicals [26], respectively (Fig. 4b). Cl and S come from the dopant acid and evocating agent. The Co 2p spectrum consists of two peaks at 780.6 eV and 795.8 eV (Fig. 4c). We can see that the binding energy difference of the two peaks is 15.2

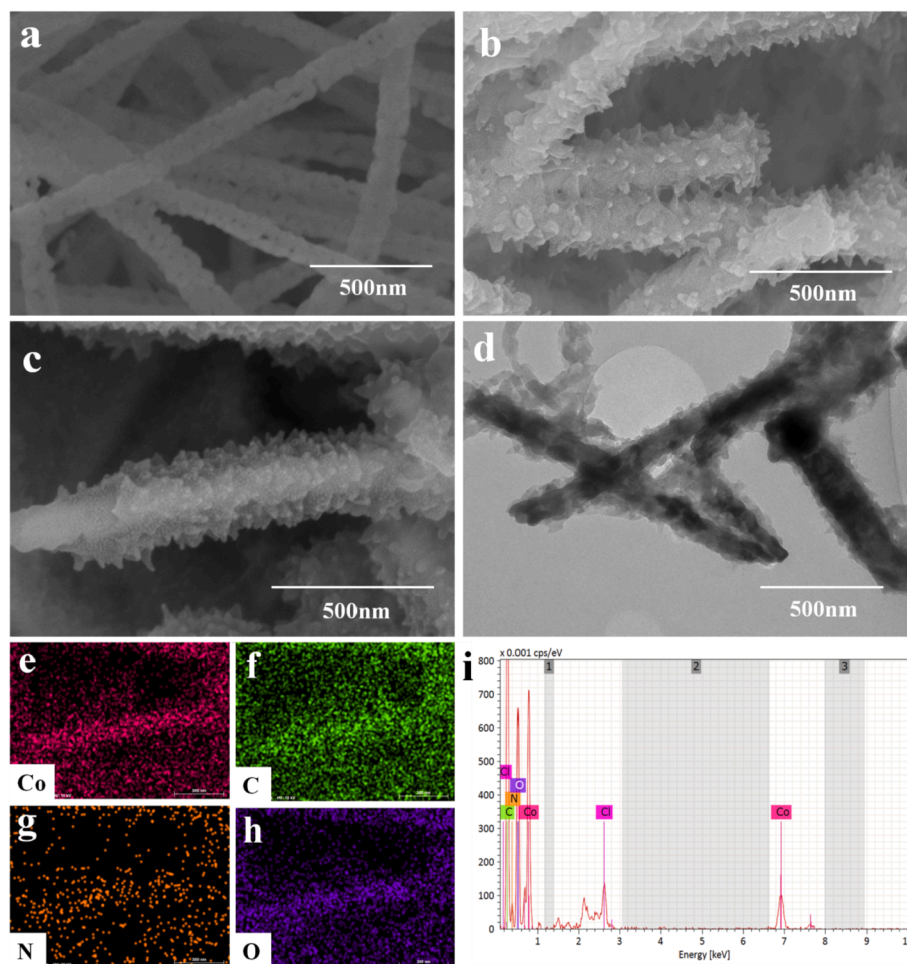


Fig. 3. SEM of Co₃O₄ (a) and Co₃O₄/PANI (1:5) (b,c), TEM of Co₃O₄/PANI (1:5) (d), elemental mapping of Co (e), C (f), N (g), O (h), and EDS spectrum of Co₃O₄/PANI (1:5) (i).

Table 1

Granularity testing results of Co₃O₄/PANI (1:3, 1:5, 1:8, 1:10).

Name	Effective diameter(nm)
Co ₃ O ₄ /PANI(1:3)	984.05
Co ₃ O ₄ /PANI(1:5)	1096.79
Co ₃ O ₄ /PANI(1:8)	3070.93
Co ₃ O ₄ /PANI(1:10)	4935.00

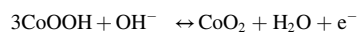
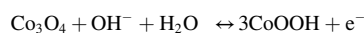
eV, and the intensity ratio of them is about 2:1. They are described as the spin-orbit-split doublet (Co 2p_{3/2} and Co 2p_{1/2}, respectively) of Co₃O₄ [27]. These are consistent with the previous characterization.

3.5. Brunauer–emmett–teller (BET)

Fig. 5 shows that the isotherm adsorption-desorption curve of Co₃O₄/PANI (1:5) belongs to the type III defined by IUPAC. The adsorption average pore diameter (4V/A by BET) is 26.4 nm, corresponding to a specific surface area of 26 m²/g. Especially, the data shows the sample having a high mesoporous ratio of 43%, which is beneficial to shorten the diffusion path of electrolyte ions and facilitate electron exchange, thus enhancing the capacitive performance of the sample [28].

3.6. Electrochemical tests

Fig. 6a shows the discharge curves of Co₃O₄ and Co₃O₄/PANI (1:3, 1:5, 1:8, 1:10) samples at 1 A g⁻¹ in GCD. The specific capacitances of Co₃O₄ and Co₃O₄/PANI (1:3, 1:5, 1:8, 1:10) have been calculated by formula (1), which are 417.8, 824, 1124, 314 and 340 F g⁻¹, respectively. Obviously, Co₃O₄/PANI (1:5) has the highest value, and Co₃O₄/PANI (1:3) ranks the second. The other samples do not perform well because they either contain too much PANI, or only cobalt oxide. Fig. 6b is the CV curves of all samples. There are two pairs of peaks in the CV curve of Co₃O₄, which show the pseudo-capacitance characteristic caused by redox reaction. The peaks are related to the transformation of different cobalt valence states. The redox reactions can be described as follows [29]:



As shown in Fig. 6c, the specific capacitance of Co₃O₄/PANI (1:5) is further measured at different current density of 1, 2, 5, 10 and 20 A g⁻¹, respectively, and the corresponding value is 1124, 964, 906, 802 and 688 F g⁻¹. Fig. 6d is the CV curves of the sample. It can be observed that the shift of oxidation peak and reduction peak happens as the increase of scanning rate, which should be caused by electrode resistance. In Fig. 6d, a pair of oxidation-reduction peaks can be observed clearly, but the other two peaks, which correspond to Co³⁺ ↔ Co⁴⁺, could only be

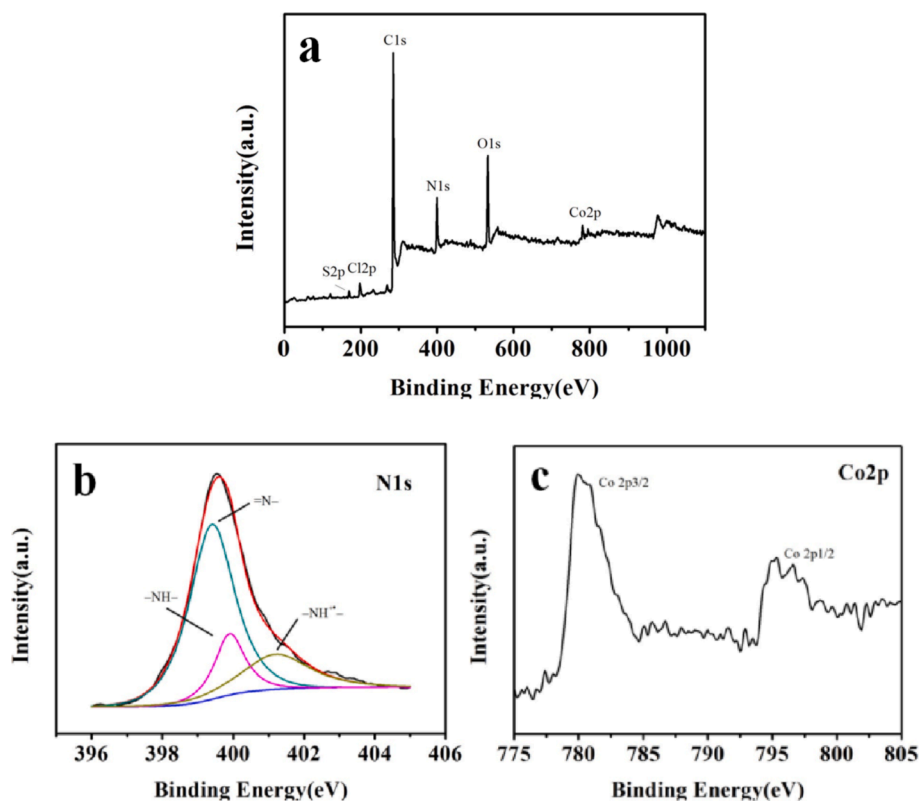


Fig. 4. XPS spectra of $\text{Co}_3\text{O}_4/\text{PANI}$ (1:5): Full spectrum (a), high resolution scan of N 1s (b) and Co 2p (c).

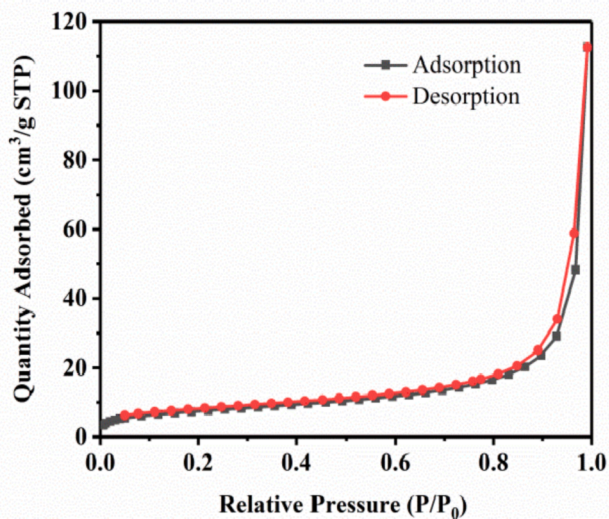


Fig. 5. Nitrogen adsorption-desorption isotherms of $\text{Co}_3\text{O}_4/\text{PANI}$ (1:5).

seen at the high scan rate. The result indicates that the addition of PANI further stimulates the redox reaction of $\text{Co}^{2+} \leftrightarrow \text{Co}^{3+}$, which causes another pair of weak peaks from $\text{Co}^{3+} \leftrightarrow \text{Co}^{4+}$ to be hidden.

The EIS spectra of all samples are shown in Fig. 6e. The intersection between the curve and the X axis is the solution resistance (R_s) at the interface between the electrolyte and the electrode. The incomplete semicircle in the high frequency region represents the electron transfer resistance of the induced charge. The slope of the line in the low

frequency region shows the diffusivity of the material. The R_s of all composite samples are all about 0.5Ω , while that of Co_3O_4 is 0.72Ω . It shows that the addition of PANI can improve the conductivity of the composites. As far the diffusion resistance, $\text{Co}_3\text{O}_4/\text{PANI}$ (1:5) has the largest slope, meaning its good diffusion performance.

The retention rate of $\text{Co}_3\text{O}_4/\text{PANI}$ (1:5) is measured. Under the current density of $5 \text{ A} \cdot \text{g}^{-1}$, there is 82.19% of the specific capacitance left after 2000 charge-discharge cycles. Extending the cycle times to 5000 cycles, the retention rate becomes 73.97%. The decrease may be ascribed to the cubical dilatation of macromolecular chains of PANI due to the insertion-release of ions in the charge-discharge cycles. It is should be pointed that pure PANI as electrode only remains 73.9% after 2000 cycles.

Fig. 6g shows the Tafel curves of Co_3O_4 and $\text{Co}_3\text{O}_4/\text{PANI}$ (1:5) in 6 mol L^{-1} KOH. Their self-corrosion potential and corrosion current are shown in Table 2. The higher the self-corrosion potential, the smaller the corrosion current, the better the corrosion resistance of the material. This shows that the coating of PANI can improve the corrosion resistance of the composites.

4. Conclusions

Co_3O_4 nanofibers are firstly prepared by electrospinning, and then $\text{Co}_3\text{O}_4/\text{PANI}$ composites are synthesized by the in-situ polymerization method. Electrochemical tests show that the performance of $\text{Co}_3\text{O}_4/\text{PANI}$ (1:5) is significantly better than that of other samples, including pure nano- Co_3O_4 , $\text{Co}_3\text{O}_4/\text{PANI}$ (1:3), (1:8) and (1:10) samples etc. Its specific capacitance is $1124 \text{ F} \cdot \text{g}^{-1}$ at the current density of $1 \text{ A} \cdot \text{g}^{-1}$. Its capacitance retention is 82.19% after 2000 charge-discharge cycles at $5 \text{ A} \cdot \text{g}^{-1}$, which still retains more than 70% after 5000 cycles. It can be deduced that only when cobalt oxide nanofibers are coated with proper amount of PANI, can the beneficial synergistic effect be realized well between the two components in the composites. The synergy here is reflected in good conductivity, ion diffusivity and high redox efficiency.

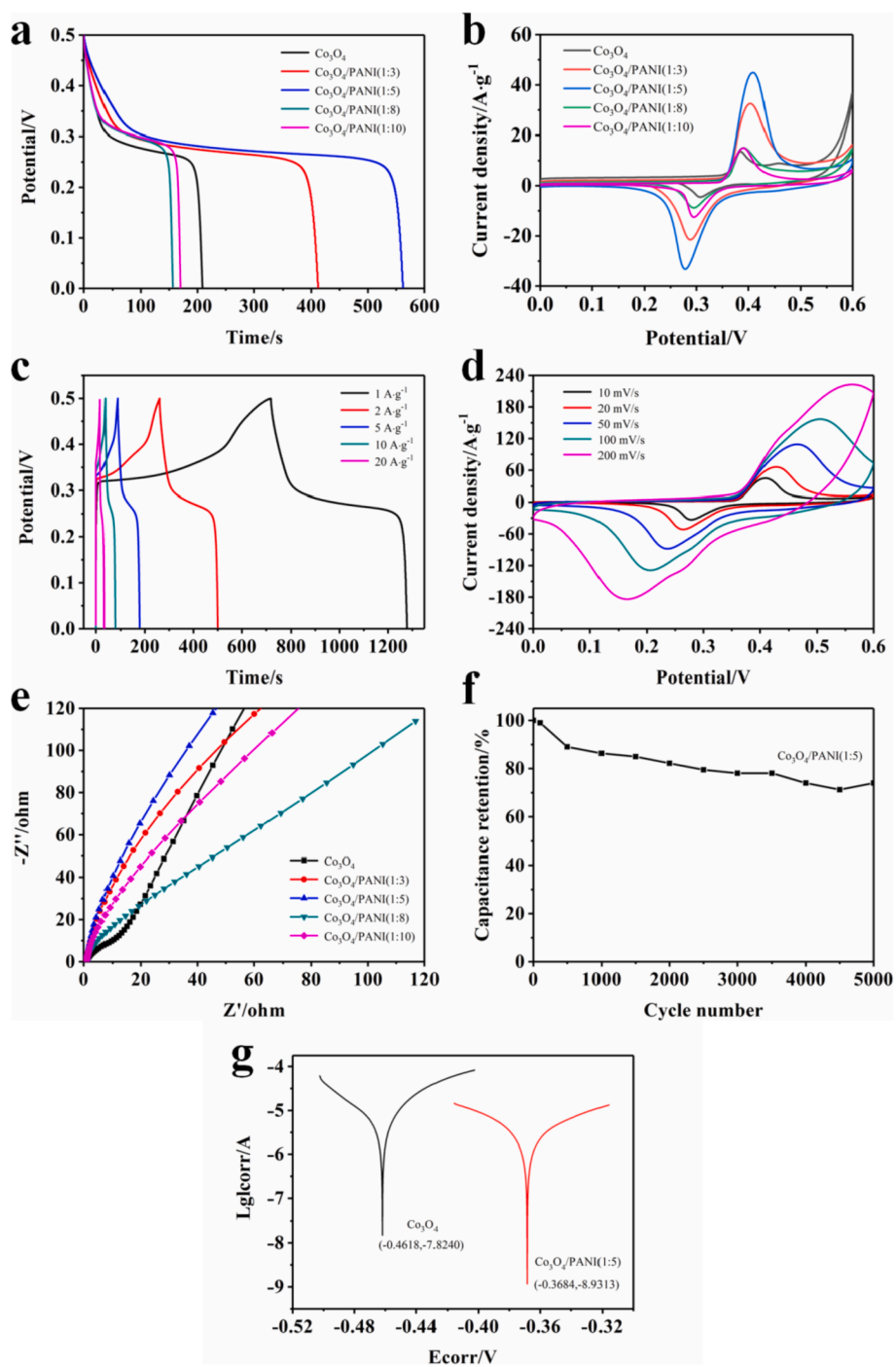


Fig. 6. GCD curves of Co_3O_4 and $\text{Co}_3\text{O}_4/\text{PANI}$ (1:3, 1:5, 1:8, 1:10) (a), CV curves of all samples (b), GCD curves of $\text{Co}_3\text{O}_4/\text{PANI}$ (1:5) (c), CV curves of $\text{Co}_3\text{O}_4/\text{PANI}$ (1:5) (d), EIS spectra of all samples (e), Cyclical stability curve of $\text{Co}_3\text{O}_4/\text{PANI}$ (1:5) (f) and Tafel curves of Co_3O_4 and $\text{Co}_3\text{O}_4/\text{PANI}$ (1:5) (g).

Table 2
Corrosion resistance of Co_3O_4 and $\text{Co}_3\text{O}_4/\text{PANI}$ (1:5).

Name	$E_{\text{corr}}(\text{V})$	$\text{Lg } I_{\text{corr}}(\text{A})$
Co_3O_4	-0.4618	-7.8240
$\text{Co}_3\text{O}_4/\text{PANI}(1:5)$	-0.3684	-8.9313

Acknowledgements

This research is supported by “the Fundamental Research Funds for the Central Universities (No. 2019XKQYMS21)”.

References

[1] B.E. Conway, *Electrochemical Supercapacitors: Scientific Fundamentals and Technological Applications*, Kluwer Academic/Plenum Publishers, New York, 1999, pp. 1–8.

- [2] D.P. Dubal, H. Lee, J.G. Kim, Porous polypyrrole clusters prepared by electropolymerization for a high performance supercapacitor, *J. Mater. Chem.* 22 (2011) 3044–3052.
- [3] R. Gottam, R.S. Bhosale, P. Srinivasan, Polyaniline salt containing dual dopants, pyrelenediimide tetracarboxylic acid, and sulfuric acid: fluorescence and supercapacitor, *Appl. Polym. Sci.* 134 (2017) 45456.
- [4] P. Wang, H. Liu, Y. Xu, Supported ultrafine ruthenium oxides with specific capacitance up to 1099 F·g⁻¹ for a supercapacitor, *Electrochim. Acta* 194 (2016) 211–218.
- [5] X. Xia, J. Tu, Y. Mai, Self-supported hydrothermal synthesized hollow Co₃O₄ nanowire arrays with high supercapacitor capacitance, *J. Mater. Chem.* 21 (2011) 9319–9325.
- [6] Y. Lei, M. Gan, L. Ma, Synthesis of nitrogen-doped porous carbon from zeolitic imidazolate framework-67 and phenolic resin for high performance supercapacitors, *Ceram. Int.* 43 (2017) 6502–6510.
- [7] X. Cao, Y. Shi, W. Shi, Preparation of novel 3D graphene networks for supercapacitor applications, *Small* 7 (2011) 3163–3168.
- [8] I. Grygorchak, R. Shvets, I.V. Kityk, A.V. Kityk, R. Wielgosz, O. Hryhorchak, I. Shchur, Photosensitive carbon supercapacitor: cavitated nanoporous carbon from iodine doped β-cyclodextrin, *Physica E* 108 (2019) 164–168.
- [9] W. Liu, Y. Zhu, Z. Chen, Multilayer black phosphorus exfoliated with the aid of sodium hydroxide: an improvement in electrochemical energy storage, *J. Electron. Mater.* 47 (2018) 4793–4798.
- [10] S. Zhang, Y. Zhu, C. Kong, Adjustment of Nickel Cobalt Sulfide morphology with double solvents for its excellent charge-discharge performance, *Mater. Sci. Semicond. Process.* 93 (2019) 99–104.
- [11] W.Y. Li, L.N. Xu, J. Chen, Co₃O₄ nanomaterials in lithium-ion batteries and gas sensors, *Adv. Funct. Mater.* 15 (2005) 851–857.
- [12] J. Jansson, A.E.C. Palmqvist, E. Fridell, On the catalytic activity of Co₃O₄ in low-temperature CO oxidation, *J. Catal.* 211 (2002) 387–397.
- [13] N. Padmanathan, S. Selladurai, K.M. Razeeb, Ultra-fast rate capability of a symmetric supercapacitor with a hierarchical Co₃O₄ nanowire/nanoflower hybrid structure in non-aqueous electrolyte, *RSC Adv.* 5 (2015) 12700–12709.
- [14] T. Liu, L. Zhang, W. You, Core-Shell nitrogen-doped carbon hollow spheres/Co₃O₄ nanosheets as advanced electrode for high-performance supercapacitor, *Small* 14 (2018) 1702407.
- [15] Y. Wang, T. Zhou, K. Jiang, Reduced mesoporous Co₃O₄ nanowires as efficient water oxidation electrocatalysts and supercapacitor electrodes, *Adv. Energy Mater.* 4 (2014) 1400696.
- [16] W. Quan, Y. Xu, Y. Wang, S. Meng, D. Jiang, M. Chen, Hierarchically structured Co₃O₄@ glucose-modified LDH architectures for high-performance supercapacitors, *Appl. Surf. Sci.* 488 (2019) 639–647.
- [17] T. Liu, L. Zhang, W. You, J. Yu, Core-Shell nitrogen-doped carbon hollow spheres/Co₃O₄ nanosheets as advanced electrode for high-performance supercapacitor, *Small* 14 (2018) 1702407.
- [18] L. Haghighi Poudeh, I. Letofsky Papst, F.C. Cebeci, Y. Menciloglu, M. Yildiz, B. Saner Okan, Facile synthesis of single and multi-layer graphene/Mn₃O₄ integrated 3D urchin-shaped hybrid composite electrodes by core-shell electrospinning, *ChemNanoMat* 5 (2019) 792–801.
- [19] H. Bigdeli, M. Moradi, S. Borhani, E.A. Jafari, S. Hajati, M.A. Kiani, One-pot electrochemical growth of sponge-like polyaniline-intercalated phosphorus-doped graphene oxide on nickel foam as binder-free electrode material of supercapacitor, *Physica E* 100 (2018) 45–53.
- [20] J. Lei, Y. Zhu, Z. Chen, Improving the electrochemical performance of Nano-PANI by adding manganese, *J. Mater. Sci. Mater. Electron.* 29 (2018) 12366–12372.
- [21] B.S. Singu, S. Palaniappan, K.R. Yoon, Polyaniline-nickel oxide nanocomposites for supercapacitor, *J. Appl. Electrochem.* 46 (2016) 1039–1047.
- [22] X. Cao, B. Zheng, W. Shi, Reduced graphene oxide-wrapped MoO₃ composites prepared by using metal-organic frameworks as precursor for all-solid-state flexible supercapacitors, *Adv. Mater.* 27 (2015) 4695–4701.
- [23] X. Wang, J. Deng, X. Duan, Crosslinked polyaniline nanorods with improved electrochemical performance as electrode material for supercapacitors, *J. Mater. Chem.* 2 (2014) 12323–12329.
- [24] Y. Hao, L. A Sani, T. Ge, Phytic acid doped polyaniline containing epoxy coatings for corrosion protection of Q235 carbon steel, *Appl. Surf. Sci.* 419 (2017) 826–837.
- [25] Y. Liu, G. Zhu, B. Ge, Concave Co₃O₄ octahedral mesocrystal: polymer-mediated synthesis and sensing properties, *CrystEngComm* 14 (2012) 6264–6270.
- [26] M. Chen, M. Wang, Z. Yang, High performance and durability of order-structured cathode catalyst layer based on TiO₂@PANI core-shell nanowire arrays, *Appl. Surf. Sci.* 406 (2017) 69–76.
- [27] M. Pal, R. Rakshit, A.K. Singh, Ultra high supercapacitance of ultra small Co₃O₄ nanocubes, *Energy* 103 (2016) 481–486.
- [28] G. Gryglewicz, J. Machnikowski, E. Lorenc-Grabowska, Effect of pore size distribution of coal-based activated carbons on double layer capacitance, *Electrochim. Acta* 50 (2005) 1197–1206.
- [29] S.K. Meher, G.R. Rao, Ultralayered Co₃O₄ for high-performance supercapacitor applications, *J. Phys. Chem. C* 115 (2011) 15646–15654.